Republic of Iraq
Ministry of Higher Education and Scientific Research
University of Diyala
College of Science
Department of Physics

Development and characterization of PANI-Iron, Cobalt, and Manganese oxides nanocomposities for gas sensing and photodetection applications

A Thesis
Submitted to the Council of the College of Science - University of Diyala in Partial Fulfillment of the Requirements for the Degree of Doctor of Philosophy of Science in Physics

By

Mehdi Hatem Diwan

B. Sc. in Physics, (1999)
M. Sc. in Physics, (2002)

Supervised By

Prof. Dr.
Nabeel A. Bakr

Prof. Dr.
Isam M. Ibrahim

2025 A. D

1446 A. H

Abstract

In this study, polyaniline nanofibers (PAni NFs) and magnetite nanoparticles (Fe_3O_4 NPs) were synthesized using the hydrothermal technique, while was employed to synthesize tetramanganese oxide nanoparticles (Mn_3O_4 NPs) and cobalt oxide nanoparticles (Co_3O_4 NPs) where synthesized via a simple precipitation method. Moreover, PAni NFs and PAni-Metal Oxide (MO) nanocomposite films were prepared using the spin-coating method. Different concentrations of PAni NFs were combined with each type of MO NPs, and the resulting films were deposited on glass as well as on n-type and p-type silicon substrates.

The structural properties using X-ray diffraction confirmed the crystalline nature of PAni NFs and the polycrystalline structures of MO NPs, with the tetrahedral Hausmannite phase for Mn_3O_4 NPs and the face-centered cubic spinel phase for Co_3O_4 NPs, as well as the cubic inverse spinal phase for magnetite. In addition, the FE-SEM showed a fiber-like morphology for PAni with diameters of (46–81) nm and a spherical nanoparticle clusters with diameters of (34-53) nm, (20–26) nm, and (58–86) nm for Mn_3O_4, Co_3O_4, and Fe_3O_4 respectively. Additionally, PAni-MO nanocomposites revealed a fiber-like shape coated with nanoparticles have a diameter of (33–53) nm, (33–46) nm, and (27–46) nm for PAni-Mn_3O_4 nanocomposites, PAni-Co_3O_4 nanocomposites, and PAni-Fe_3O_4 nanocomposites respectively.

The UV-Vis spectrum of PAni NFs revealed two absorption peaks at 296 nm and 627 nm, corresponding to π-π^* electronic transitions in the benzenoid ring and electron transitions in the polymeric chain from benzenoid to quinoid rings, respectively. However, the shift of peaks toward higher wavelengths for PAni-MO nanocomposites highlighted the decrease in the energy gap in PAni nanocomposites. The FT-IR spectra

Abstract:

emphasized the formation of PAni NFs and MO NPs. The red-shifted peak positions in PAni-MO nanocomposites also showed that PAni NFs and MO NPs strongly interacted with each other.

Electrical properties were investigated through D.C and A.C conductivity measurements. However, the D.C. conductivity tests of PAni NFs and PAni-MO nanocomposites films showed that as the temperature increased, the D.C. conductivity increased as well. Moreover, the activation energy calculations confirmed an increase in the D.C. conductivity of PAni nanocomposites with increasing MO NPs content. The A.C. conductivity tests showed an increase in A.C. conductivity for PAni NFs and their nanocomposite films as the frequency increased from (50 Hz to 3 MHz). Additionally, the A.C. conductivity increased as the MO content in PAni nanocomposites increased in comparison to PAni NFs. The dielectric behaviour of PAni NFs and their nanocomposites showed that both the dielectric constant and the loss factor decreased as the frequency increased. The investigations showed that the dielectric constant and the loss factor also increased as the metal oxide content in the polymeric matrix increased.

Hall effect measurements proved that PAni NFs, Co_3O_4 NPs, and PAni-Co_3O_4 nanocomposites behaved as p-type semiconductors. In contrast the Mn_3O_4 NPs and Fe_3O_4 NPs, as well as the other PAni-Mn_3O_4 and PAni-Fe_3O_4 nanocomposites behaved as n-type semiconductors. The C-***V*** characteristics showed that the capacitance decreases as the reverse bias voltage increases for PAni, MO NPs, and PAni-MO heterojunction devices. The capacitance also decreased as the MOs content in the PAni nanocomposite films increased. Moreover, the linear portion of the $1/C^2$–***V*** plot confirmed the abrupt heterojunction between PAni NFs and their nanocomposite films with p-type and n-type silicon substrates. In

Abstract:

addition, the results showed a decrease in the built-in potential (V_b) values with an increase in the MO NPs content within the polymer matrix.

The I-***V*** curves in both dark and light conditions showed that the photocurrent increased as the light intensity and MO NPs in the PAni nanocomposites increased which support the photodiode behaviour. Moreover, the ideality factor values confirmed the non-ideality behaviour of the prepared photodiodes. The I-t curve for each ON/OFF pulse of the prepared heterojunction devices was conducted under various wavelengths (300–500 nm), which revealed an increase in photocurrent with each illumination pulse. Moreover, the results demonstrated an increase in photocurrent as the content of MO NPs in PAni nanocomposites increased.

The gas sensing properties revealed an increase in their sensitivity when exposing the prepared films to NH_3 gas. It is clear that the PAni-MO nanocomposites at the concentrations of 5 mL PAni-5 mL Co_3O_4 and 5 mL PAni-5 mL Fe_3O_4 have yielded the highest sensitivity values, measuring 20.5% and 18.49%, respectively, compared to the other sensitivity values of the PAni nanocomposite films. Moreover, the results reveal also that the Co_3O_4 NPs and Fe_3O_4 NPs films outperformed the other samples, exhibiting the highest sensitivity (646.39%) and (166.36), respectively.

Chapter One
Introduction and Basic Concepts

1.1 Introduction

Polymers are crucial due to their widespread use in all human activities. They are multi-functional materials and are gradually replacing glass, paper, metals, and other common materials in all application types because of their flexibility, light weight, and cheapness [1]. Many polymeric applications employ systems consisting of a mixture of multiple polymer components and additives rather than relying solely on a single chemical component. The process of incorporating different minerals and inorganic material additives results in different types of products, each with unique physical properties and low costs [2].

Scientific research has demonstrated that filler size in fiber-reinforced composites directly and significantly affects material properties, largely determining surface interactions related to adhesion, particle movement, and dispersion as well as the bonds between the matrix and the surface [3]. Reducing the filler's particle size to the nanoscale significantly changes many properties. These properties included electrical characteristics, catalytic activity, and gas adsorption. Materials whose one dimension is at least in the size range from 1 to 100 nanometers are known as nanomaterials [4].

Nanomaterials in general are different from macroscopic and bulk materials due to their qualitative distinction and the presence of many unusual, interesting, and useful features [5]. The majority of the nanomaterial's characteristics depend on several factors, including size, shape, and surface structure.

Polymer nanocomposites (PNCs) are usually described as mixtures of polymers and nanomaterials that have at least one dimension and one material that is in the nanometer range, which is less than 100 nm in size. However, the process of combining nanomaterials in the polymer matrix

aims to improve many other original polymer properties, including biodegradability, heat resistance, and mechanical properties, in addition to creating new ones through uniform nanomaterial dispersion [6]. In 1970, Thing first proposed polymeric nanocomposites [7]. Many academic laboratories and commercial research institutions continued to develop nanocomposite materials until the late 1980s [8, 9]. The extensive published research reflects the significant progress technological companies have made in developing nanocomposites in various application fields.

The combination of nanomaterials with a polymer host matrix significantly changes the physical, chemical, and surface properties of polymer nanocomposites. Additionally, it alters other factors, such as size, the ratio of surface area to volume, surface chemistry, and geometry, all of which significantly impact the performance of polymer nanocomposites. Polymeric nanocomposites, a new category of materials with unique properties, have surpassed traditional composites and doped polymer systems. In general, nanocomposites are different from their regular counterparts because nanomaterials interact with polymer surfaces in a polymer matrix on a nanoscale.

Among the conducting polymers, polyaniline has attracted considerable interest in recent years because of its suitable electrical, optical, and electrochemical properties as well as its high stability and wide applications in microelectronic devices, diodes, batteries, supercapacitors, electromagnetic shielding, sensors, etc. However, to obtain materials with synergetic behavior between PAni and inorganic nanoparticles, various nanocomposites of PAni with inorganic nanoparticles have been synthesized in recent years, such as Mn_3O_4, Mn_3O_4, Fe_3O_4, etc. These nanocomposites exhibit enhanced physical

properties through the abundance of the interfaces and the extent of the dispersion of fine particles within polymer matrices [10].

1.2 Nanotechnology

Nanotechnology is an advanced science that involves the design, production, characterization, and application of advanced materials based on the nanoscale [11]. Taniguchi first discovered the term nanotechnology in 1974, defining it as the science of nanomaterials (1-100 nanometers), demonstrating that systems with nanoscale structures and components exhibited physical, thermal, and chemical properties. The literature has shown that nanofillers used in materials led to significant improvements in electrical, mechanical, thermal, optical, and barrier properties [12]. The field of nanoscience and nanotechnology has flourished over the past decades and has become important in many applications such as biosensors, nanomedicine, aeronautics, computing, polymer modification, and many other broad fields due to its large surface area ratio to the size it provides in improving and modifying the properties of materials [13].

1.3 Nanofillers

The term nano is defined as an item on the nanometer scale (10^{-9} m). An additive agent is a nanofiller that is dispersed in the polymeric matrix of a compound with at least one dimension on the nanoscale [14]. Nanofiller materials currently used, whether from natural or synthetic sources, have received considerable attention from many researchers as promising materials of the future due to the unique properties they possess compared to bulk counterparts. The nanofiller addition tends to modify or improve the variable properties of materials, which include physical, electrical, optical, mechanical, and thermal properties, and

sometimes synergizes with conventional fillers [15]. There are a wide variety of methods in the synthesis of nanomaterials, such as chemical, physical, mechanical, and biological. However, the shape and dimension of nanofillers are crucial elements in various applications. In general, nanofillers are classified into 0-D, 1-D, and 2-D materials according to their dimensions, not confined to the nanoscale (<100 nm) range [16], as depicted in Figure (1.1) [17].

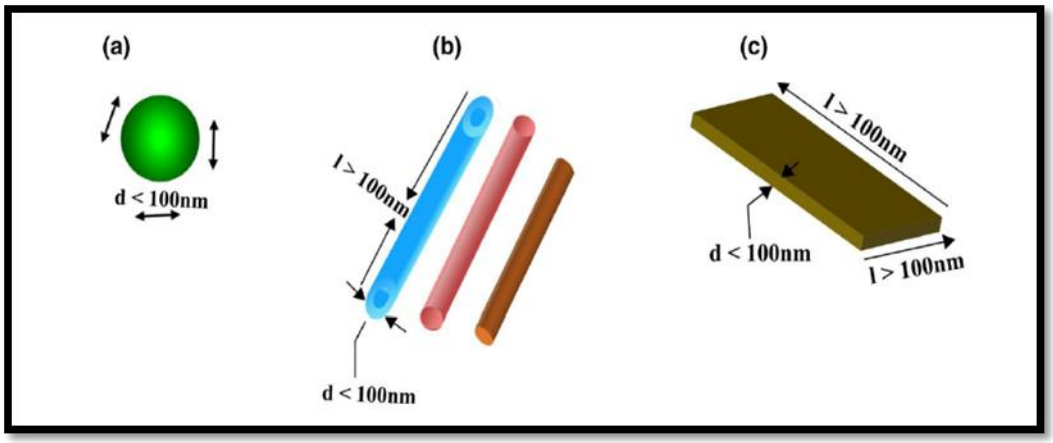

Figure 1.1: Nanofiller classification based on dimensionality: (a) 0-D (Spherical nanofiller), (b) 1-D (Nanowires and Nanorods), and (c) 2-D (Nanosheets) [17].

1.4 Nanomaterials Synthesis

Generally, three methods have been used in the synthesis of nanoparticles: physical methods, also known as top-down methods; chemical methods, also known as bottom-up methods; and biological methods, also known as the green methods [18]. Figure (1.2) shows the methods used to assemble nanoparticles [19].

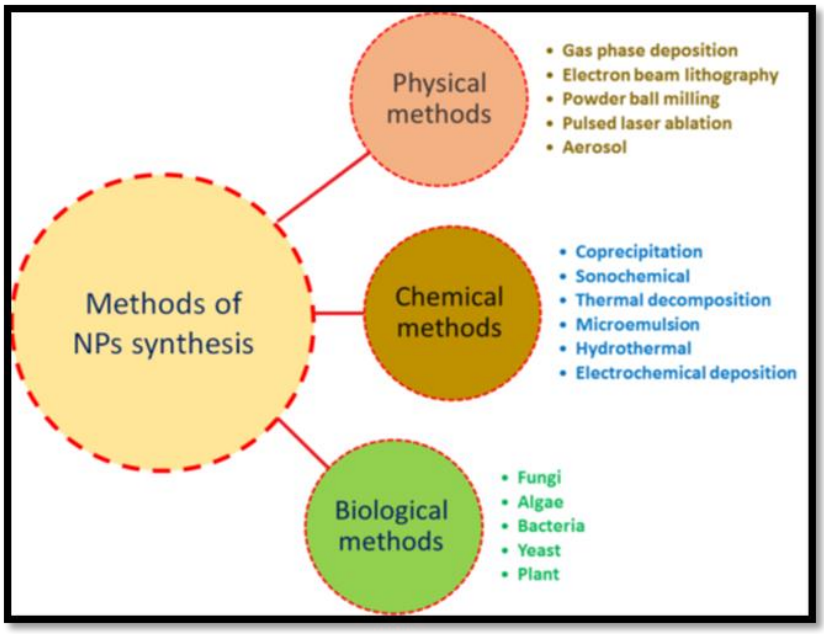

Figure 1.2: Schematic showing the nanoparticle synthesis using several processes [19].

There are two main types of chemical methods used in nanoparticle synthesis: the sedimentation method and the reduction method [20]. Figure (1.3), subdivides each of them into several different methods. The current study employed both chemical precipitation and hydrothermal methods in the nanoparticle synthesis.

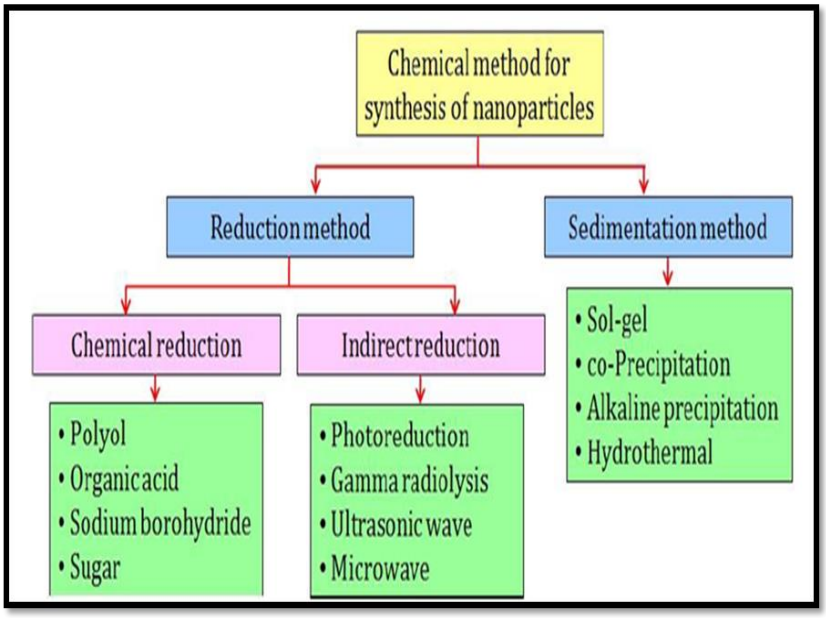

Figure 1.3: Schematic diagram showing the various types of chemical methods used in nanoparticle synthesis [21].

1.4.1 Hydrothermal (or solvothermal) method

The hydrothermal method can produce a variety of morphologies through its reactions, enabling heterogeneous nucleation and growth under high-temperature and high-pressure conditions compared to ambient conditions [22]. However, hydrothermal process can be defined as any chemical reaction that can occur in the presence of a solvent (it can be aqueous or non-aqueous), at a temperature and pressure lower than the solvent's critical point, and under supercritical conditions in a closed system (autoclave) [23]. The process can occur in the presence of liquid, and one of its advantages is its ability to form compositions and morphologies that are difficult to obtain under ambient conditions. Moreover, by adjusting the nucleation rate and growth, controlling both temperature and time, and selecting the reactants, one can obtain the chemical and physical properties based on the morphologies and compositions [22]. Frank studied the water properties under hydrothermal conditions and he showed that they are changed with the viscosity (liquid molecular mobility), the molten salt, and the dielectric constant, which dissociates into H_3O^+ and OH^- [24]. Under normal conditions, these abnormalities do not form the resulting materials in any way. Figure (1.4) presents a schematic diagram that illustrates the process of preparing nanomaterials using the hydrothermal method.

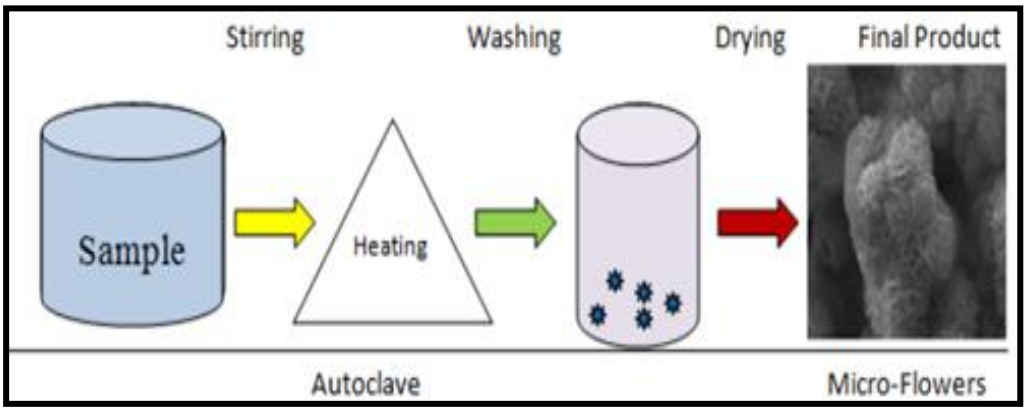

Figure 1.4: Schematic showing the hydrothermal process [25].

1.4.2 Chemical Co-precipitation method

The chemical co-precipitation method in solution, or the so-called wet chemical method, is one of the common methods in the multi-component ceramic material synthesis.

This method simultaneously separates the insoluble precipitate mixture, consisting of two or more substances from the solution [26]. This method primarily uses mineral salts such as nitrates, chlorides, sulphates, and others as precursors, which dissolve in water and other suitable liquids to create a uniform solution of ionic clusters. The solution undergoes evaporation and pH changes, which serves as effective and influential factors in the deposition process of salts (hydroxides or oxalates). Salt concentration and true pH, as well as the change rate of pH and temperature, are factors that have a significant impact on crystal growth and agglomeration [27]. Once the precipitation process is complete, then the precipitate is collected, washed, and dried by gradually heating it to the boiling point. However, the washing and drying process of hydroxide directly influences the final powder agglomeration degree. Therefore, this method aims to synthesize nanopowders with a crystalline structure from typically amorphous compounds, particularly those synthesized at low temperatures. Consequently, this method requires heat treatment [28].

The calcination process typically converts hydroxides into crystalline oxides. A high-pressure hydrothermal reactor is often used for calcination or hydrothermal treatment to complete the crystallization process in most systems with one, two, or three components [29].

The homogeneous reactions have several advantages: The homogeneous component distribution, relatively low reaction heat, low particle agglomeration density, and low cost are all advantages of

homogeneous reactions. The reactions that occur in the co-precipitation process generally depend on the reaction conditions. Therefore, incomplete metal ion deposition poses significant challenges in controlling the stoichiometry of the chemical elements used as precursors. Furthermore, certain oxide/hydroxide materials, such as those in amphoteric systems, are not suitable for co-precipitation reactions [30]. Figure (1.5), reveals the detailed flowchart for the synthesis of ceramic nanoparticles using the chemical precipitation method.

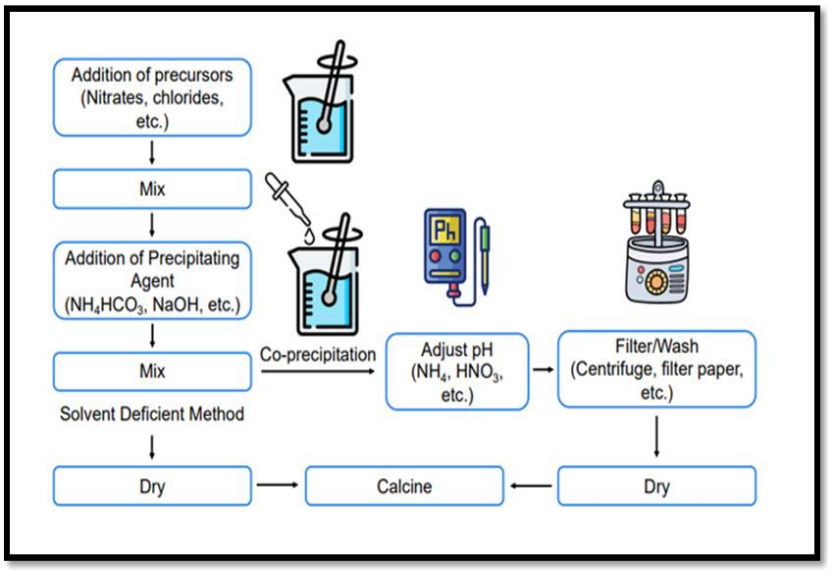

Figure 1.5: Flow chart diagram for the ceramic nanoparticle's synthesis using the chemical precipitation method [31].

1.5 Conducting polymers

Conductive polymers are a category of conjugated polymers that consist of single and double bonds alternately along the polymer chain. Protons and oxidation (p-doping) or reduction (n-doping) catalyze the doping process, which enhances the conductivity of the conducting polymer. Some of the most studied and used conductive polymers are polyaniline (PAni) and its variants, polythiophene (PTh), polypyrrole (PPy), polyacetylene (PAc), polynaphthylamine (PNA), polyphenylene phenylene (PPV), poly(3-hexylthiophene) (P3HT), polycarbazole (PCz),

and poly(3,4-ethylenedioxythiophene) (PEDOT), as depicted in Figure (1.6). The conductive polymers have been extensively studied because of their chemical and physical properties, which include environmental stability, thermal tolerance, enhanced electrical conductivity, and the ability to expand doping. Chemical polymerization processes, such as chemical oxidation or electrochemical polymerization, can be used to synthesize conductive polymers using their monomers and other cofactors [32].

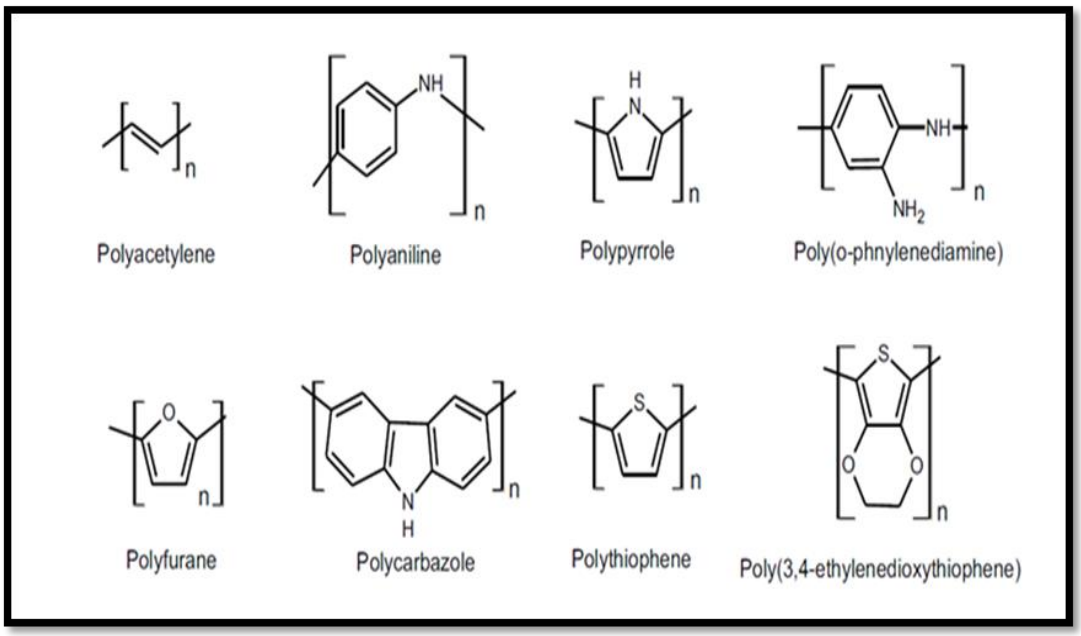

Figure 1.6: Some conducting polymer structures [32].

Optoelectronics, a field that combines electronics and optics, has shown significant interest in conductive polymers because of their adjustable properties, high-quality processes, cheapness, and flexible compatibility with other polymeric materials [33]. Many medical applications have also utilized polymers because of their charge transfer properties and biocompatibility. Conductive polymers' tunable chemical and physical properties enable the creation of various shapes and forms, including polymeric nanoparticles, thin optical films, nanofibers, and nanowires, while also enhancing their properties [34, 35]. Besides the previously

mentioned applications, conductive polymers are used in solar cells and light-emitting diodes, sensors, lasers, batteries based on lithium-ion, phototransistors, and supercapacitors.

1.6 Conduction mechanism in conductive polymers

The ability of polymers to conduct electricity is due to the π-conjugated system in their backbone, which consists of alternating single and double bonds. This lets the π-bond orbitals overlap along the polymer chain [36]. The polymer's conductivity efficiency can be controlled to achieve the desired luminance emission within a specific range, which can be achieved by reducing the energy gap separating the highest occupied molecular orbital (HOMO) and the lowest unoccupied molecular orbital (LUMO) and by stimulating the different functional groups to withdraw/release electrons in the polymer backbone. Controlling the electron-gap transfer/injection processes of the prepared polymers enables efficient use in optoelectronics [37]. However, an increase in the number of charge carriers will enhance the conductivity of the conductive polymer. The energy gap model and the quasi-one-dimensional system demonstrate the polymers' conduction processes.

In general, nonlinear, self-localized fundamental excitations like solitons, polarons, and bipolarons describe systems that are almost one-dimensional [38]. Figure (1.7) [39], illustrates the classification of conductive polymers based on their ground state degeneracy. The synthesized trans-polyacetylene is considered the first conductive polymer with a degenerate ground state, which means that the ground state energies for both chain geometries are equivalent, facilitating the interconversion of the two forms without the need for an energy barrier. However, combining the two ground states of the trans-polyacetylene will

result in the formation of a neutral soliton, a defect with a half-integral spin [40].

In general, charged solitons, whether negative or positive, are spinless. Adding dopants will lead to the production of negative and positive solitons (electron donors or electron acceptors). As the dopants increase, the number of ground states increases, resulting in the creation of a soliton band. As a result, conductive polymers that have a degenerated ground state will conduct electricity [41].

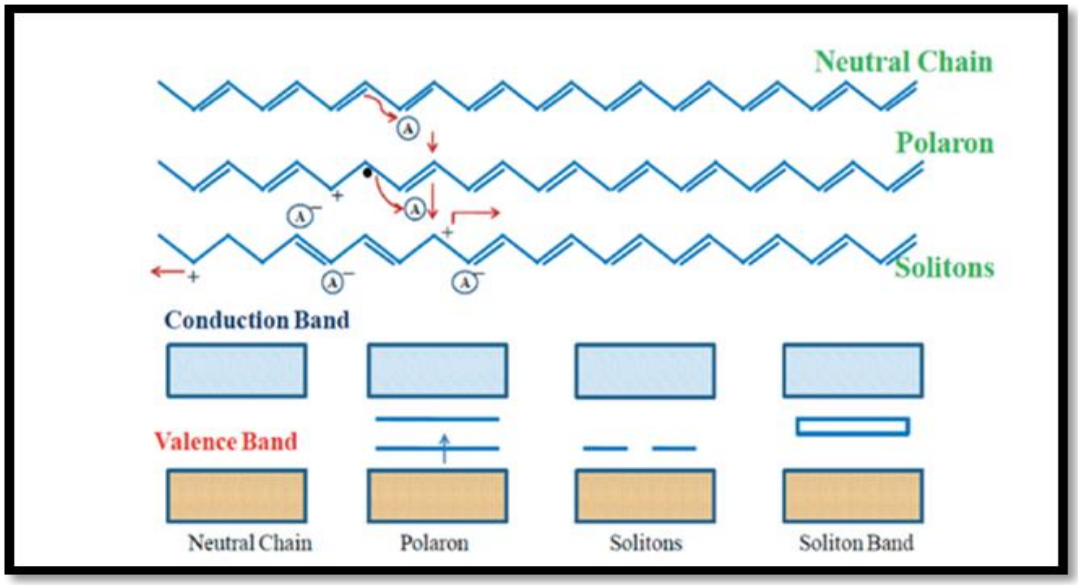

Figure 1.7: Schematic depicts the conduction mechanism and the degenerate ground states [39].

Among the widely used polymers that have non-dissolved ground states are polyaniline, polypyrrole, poly(p-phenylene), polythiophene, etc [42]. This non-degenerate nature dictates that the charged soliton will combine with the neutral anti-soliton, forming a polaron (spin 1/2). Also, when the positive soliton combines with the neutral antipart, it will form positive radical cations, or polarons, and vice versa. However, as the doping concentrations increase, neighboring polarons become closer to each other. Therefore, the two neutral solitons will form a polaron pair, leaving

charged solitons behind in the polymer chain. Ultimately, this will result in the formation of spinless, doubly charged bipolarons. Then, as the doping ratio increases, the bipolaron states will overlap more, forming what is known as a bipolaron band. However, solitons, polarons, and bipolarons are responsible for the conductive properties of these polymers [43].

1.7 Conducting Polymers Synthesis

The synthesis of electrically conductive polymers can be achieved through a variety of methods, including the following [44]:

i) Chemical polymerization

ii) Photochemical polymerization

iii) Electrochemical polymerization

iv) Concentrated emulsion polymerization

v) Methathesis polymerization

vi) Solid-state polymerization

viii) Pyrolysis

vii) Inclusion polymerization

ix) Plasma polymerization

x) Microwave polymerization

xi) Soluble precursor polymerization

The chemical polymerization technique is one of the commonly used methods of oxidative conjugation, which is used to create radical cations by oxidizing the monomers, which then conjugate to create binary cations. Consequently, the process of repetition will eventually result in the formation of the desired polymer.

1.7.1 Chemical Polymerization

Chemical polymerization is a technique with many uses in the synthesis of many types and large amounts of conductive polymers [45].

However, one can carry out the chemical synthesis process in a solution that dissolves the conducting polymer monomers and the oxidant in an acidic medium. Among the acids frequently used in the synthesis of conductive polymers are sulphuric acid (H_2SO_4), hydrochloric acid (HCl), potassium dichromate ($K_2Cr_2O_7$), ammonium persulphate ($(NH_4)_2S_2O_4$), sodium vanadate ($NaVO_3$), cerium sulphate ($Ce(SO_4)_2$), potassium iodate, hydrogen peroxide (H_2O_2), potassium ferricyanide (K_3(Fe (CN)$_6$), and some Lewis acids used as oxidizing agents [46]. However, Chemical oxidative polymerization enables the synthesis of doped and conductive states for polymers. Strong reducing agents like ammonia or hydrazine can also isolate the neutral polymer during the synthesis process. The advantages of chemical oxidative polymerization include the formation of soluble polymers through the proper substitution of aromatic and heterocyclic monomers. Conventional analytical techniques establish the primary structure of these polymers. Natural conditions of polymerization can facilitate the production of large amounts of polymer. Chemical oxidative polymerization has several disadvantages and frequently produces low-quality polymers. For example, the Lewis acid-catalyzed polymerization process, which deposits the oxidized polymer which is thought to be more rigid in the polymerizing medium, limits the degree of polymerization [47]. Furthermore, the strongly oxidizing agent's use increases the degree of oxidation, ultimately leading to the decomposition of the polymer. Another disadvantage of this method is that the solution contains a high ionic strength and an excess of oxidant, which leads to the appearance of impurities [48].

1.8 Conjugated polymers

Conjugated polymer chains, which consist of alternating single s-bonds and double s-bonds along the polymer backbone, typically couple

to conducting polymers, forming delocalized electrons in the process. Single and double molecule bonds, along with substituted groups associated with the polymeric chain atoms, lead to the formation of an extended π-orbital system. However, this system is responsible for the optical, electrical, and electrochemical properties of conjugated polymers. Therefore, through this system, electrons have the ability to move from one end of the polymer to the other [49].

1.9 Polyaniline (PAni)

Polyaniline is one of the most important categories of well-known conductive polymers. Its chemical formula is C_6H_7N. Previously referred to as black aniline, it has garnered significant attention in applied research in the last ten years because of its favorable electrical characteristics, which stem from the abundance of electrons, and its exceptional processing and modification capabilities [50]. Other PAni properties include its simple molecular structure, low cost [51], environmental stability, and its ability to dope with protonated acids [52]. In addition, it is simple to synthesize through chemical and electrochemical processes and has many applications in lithium batteries, solar cells, fuel cells, supercapacitors, sensors, etc. [53]. In general, PAni is a typical phenylene-based polymer because it contains a chemically flexible -CH_2- group in the polymer chain that is linked on both sides to a phenylene ring. The -NH- group primarily influences the protonation and deprotonation processes of PAni, along with other properties [54]. As well as, PAni is a chemical compound composed of alternating benzenoid and quinoid rings connected by a nitrogen bond. Figure (1.8) [55], depicts the PAni construction from reduced (B-NH-B-NH-)n and oxidized (B-N=Q-N=)n repeat units, where "B" denotes benzenoid and "Q" denotes

quinoid [56]. The ratio of amine to nitrogen atoms can characterize the oxidation states of PAni [57].

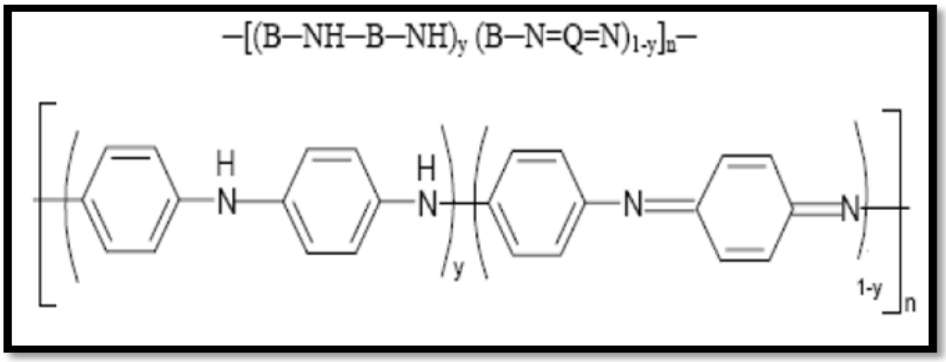

Figure 1.8: Polyaniline chain structure [55].

The fully reduced formula of PAni is leucoemeraldine when y = 1, which is usually yellow-colored and insulating. Emeraldine base (EB) is the half-oxidized state when y = 0.5; it is blue in color and insulating. The protonated form of emeraldine salt (ES), which is colorably green, is considered the only conductive state of polyaniline [58]. When y = 0, the fully oxidized form of polyaniline is obtained, known as pernigraniline base (PN), which is purple in color and insulating. Figure (1-9) displays the various oxidation states of PAni [59].

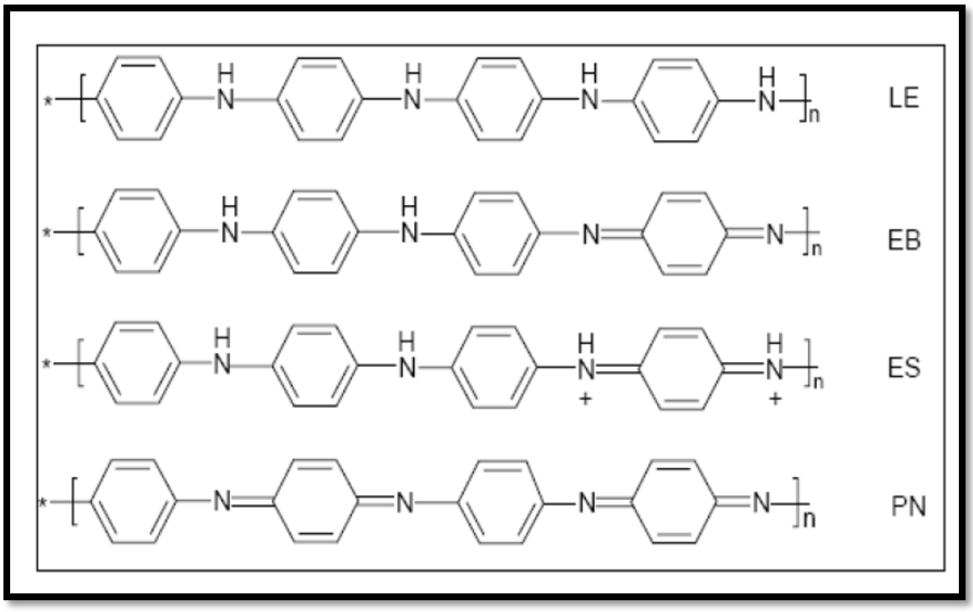

Figure 1.9: Types of oxidation states of PAni, Leucoemeraldine (LE), Emeraldine base (EB), Emeraldine salt (ES) and Pernigraniline (PN) [59].

1.9.1 PAni conductivity

Polyaniline differs from other electrically conductive polymers in its conduction mechanism due to the radical cation that forms as a result of the presence of the nitrogen atom. Therefore, it differs from other conducting polymers whose radical cation is formed as a result of the presence of the carbon atom. Moreover, nitrogen significantly contributes to the conjugated double bond system. However, polyaniline electrical conductivity depends on both protonation and oxidation degrees [60]. Polyaniline can be changed into different oxidation forms, which allows the emeraldine base form to be doped (protonated) into the emeraldine salt form, which represents the polyaniline conductive form. Generally, the half-oxidized form of the emeraldine base consists of equal amine (-NH-) and imine (=NH-) sites. The protonation process exposes the imine sites, forming the emeraldine salt, or bipolaron. The bipolarons separate by injecting an electron pair from two imine nitrogen pairs into the quinoid imine ring, which forms the third double bond of the benzenoid ring [61]. The unpaired electrons in nitrogen atoms are actually polarons and represent cationic radicals. Figure (1.10) clearly demonstrates the high polyaniline conductivity in the form of the emeraldine salt. This can be due to the polaron network, which redistributes polarons along the polymer chain. Despite the proposed theoretical models for emeraldine salt conductivity that involve polarons and bipolarons [62],

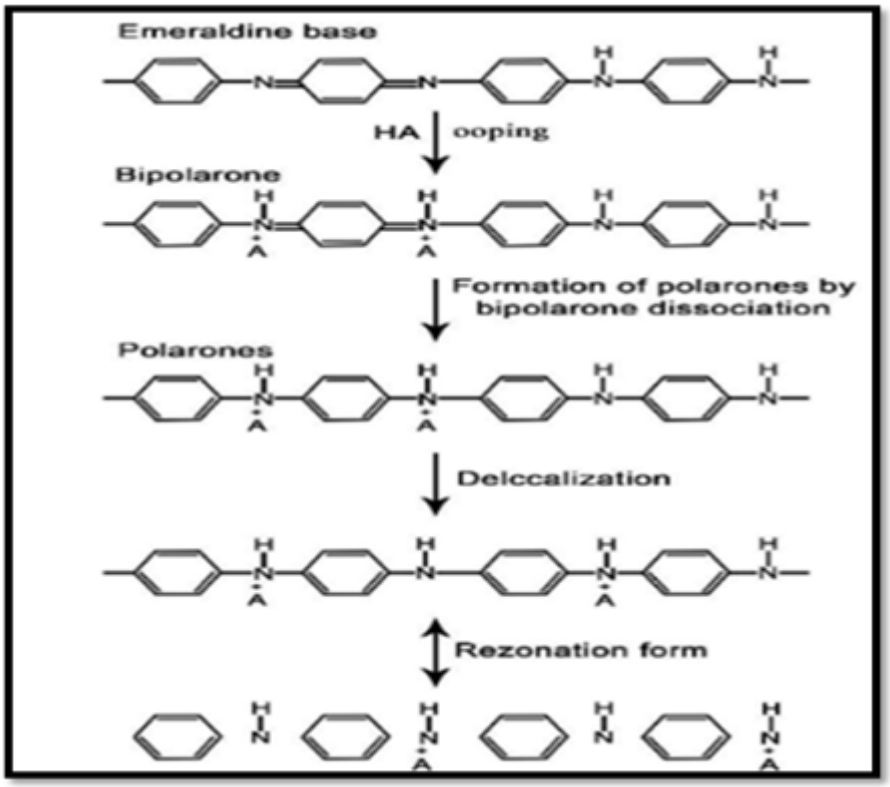

Figure 1.10: Schematic representation the polyaniline conductivity [60].

1.10 Hybrid materials

Hybrid materials are among the most technologically advanced materials because they play a significant role in creating new materials with distinctive properties; they are formed by the synergistic combination of inorganic and organic components at the molecular level. This process creates interesting materials for targeted research in chemical and physical applications. Combining properties and selecting materials most suitable for synergistic binding opens the way for a unified approach to creating substances that have the potential to solve many technological problems in the future [63]. Hybrid materials are broadly defined as synthetic materials composed of closely mixed organic-inorganic components. They can be homogeneous systems, consisting of repeating units (monomers) that combine inorganic and organic components, or they can be heterogeneous phase-separated substances, with at least one part ranging in size from a few angstroms to

several nanometers [64]. In general, hybrid materials offer superior advantages over their individual component counterparts. This is because the individual components of inorganic materials significantly contribute to the formation of hybrid materials. These components include thermal and mechanical stability, a porosity network for catalysts and sensing, a specific magnetic contribution, redox, chemical or electrochemical properties, and electronic properties. Synthetic chemists can significantly expand their matrix range by incorporating organic components. Moreover, organic materials alter the mechanical properties that enable the production of fibers and films, shape various geometric structures through casting for integrated optics, manage interconnected networks and porosity, and regulate the hydrophilic/hydrophobic equilibrium. Furthermore, organic components can specifically influence various chemical and physical properties, including optical and electrical properties, chemical or biochemical reactivity, and electrochemical behavior, among others [65].

1.11 Classification of Organic-Inorganic hybrid Materials

The preparation of hybrid materials involves two types of interactions between organic and inorganic materials during the dispersion process. Figure (1.11) illustrates the classification of hybrid materials into two categories, Class I and Class II, based on these interactions [66]. The first category of hybrid materials, which can be produced from this type of interaction between organic and inorganic materials, is the physical interaction of π-π^* (aromatic interaction), hydrogen bonding, etc. The individual components of the organic and inorganic in this category of hybrid materials are composed of specific effective functional groups that facilitate physical interaction and the formation of a homogeneous mixture between these two types of

materials. In the event that these functional groups are not present in both the organic and inorganic materials, then heterogeneity will occur between the organic and inorganic materials, which leads to phase separation, as shown in Figure (1.11) [67].

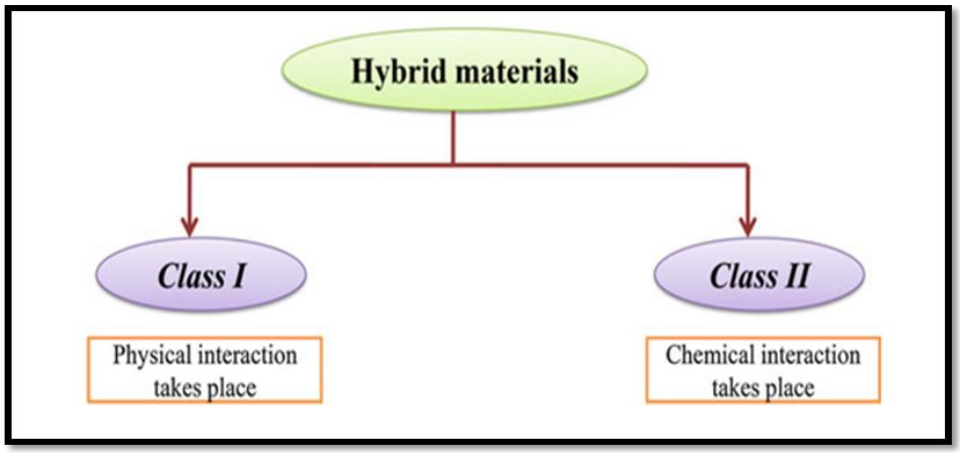

Figure 1.11: Hybrid materials classification according to organic and inorganic interaction components [63].

The presence of aromatic moieties in inorganic matrices easily generates a homogeneous mixture when there is an organic matrix containing aromatic moieties [68]. In the second category (Class II) of hybrid materials, chemical bonding typically occurs between two different phases. To do this, different methods are used. One way is to add compatibilizers, which are large molecules that mix well with other molecules, to the organic and inorganic parts. This makes the two substances mix evenly or the two different phases mix [69].

The chemist Makisima classified materials into four categories: composites, nanocomposites, hybrids, and nanohybrids as depicted in Figure (1.12) [70]. This classification refers to the dispersion of materials that form the matrix at the micron scale as composites. Mixing the materials at a scale less than a micron form nanocomposite. Hybrids, or nanohybrids, were defined by the scientist Maxima as “a mixture of different material types at the sub-micron level”. Maxima also defined

hybrids as "a mixture of different substances that exhibit chemical bonds at the molecular or atomic level" [71].

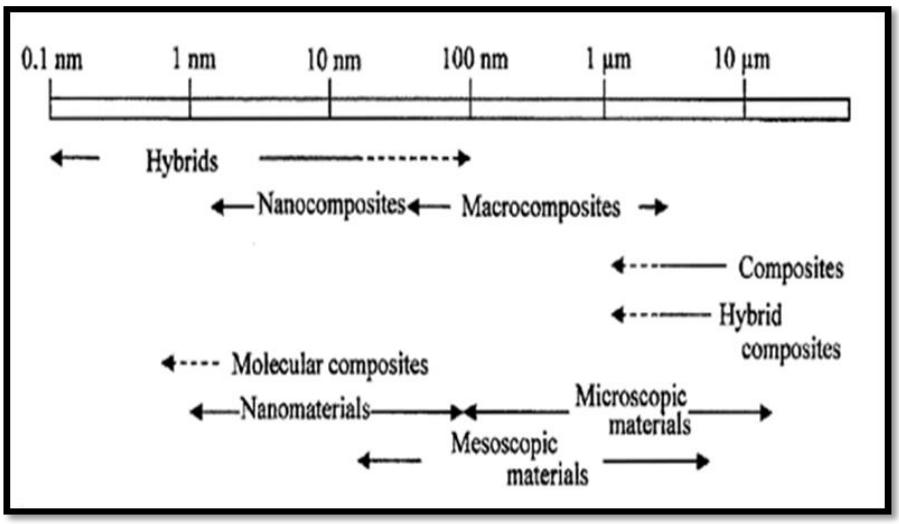

Figure 1.12: Materials classification according to the scale levels [71].

1.12 Organic-Inorganic hybrids synthesis

Hybrid organic-inorganic materials have significantly contributed to the development of numerous advanced nanomaterials. In addition to serving as an alternative to new material synthesis for academic and research purposes, hybrid materials have also played a significant role in the development and innovation of various smart materials, finding wide applications in fields such as medicine, electronics, the environment, biology, mechanics, and optics. However, researchers have employed a variety of methods to synthesize both organic and inorganic hybrid materials. The most commonly used and effective methods for preparing polymer-based hybrid materials are sol-gel, blending, emulsion polymerization, and microemulsion.

1.12.1 Blending method

There are three types of blending methods that are utilized to synthesize hybrid materials: (a) solution blending, (b) melt blending, and (c) powder blending.

(a) Solution blending

Solution-blending is considered the simplest method in the synthesis of organic-inorganic hybrid materials. This method required preparing the organic solution and dissolving it in the appropriate solvent. Subsequently, the inorganic material will be added, hence the dispersion process will be completed through stirring or ultrasonication. The hybrid material then converts to a solid state through solvent evaporation, making it easy to process. Despite its simplicity and cost-effectiveness, the disadvantage of this method is that it causes hybrid material agglomeration, which is a result of the inorganic material's agglomerating properties. Consequently, this results in the hybrid materials being produced with weak physical, mechanical, and chemical properties. Therefore, to overcome these challenges, the inorganic materials must be dispersed thoroughly, mixing them with the organic component [66].

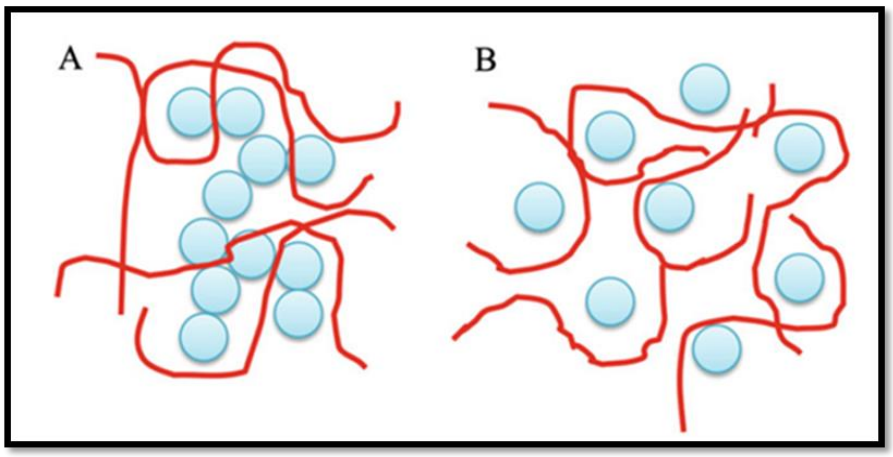

Figure 1.13: Organic- inorganic composites (A) agglomeration (B) dispersion [66].

(b) Melt blending

The melt blending method is a process that bears resemblance to the solution blending technique, but it differs in that it involves melting. Compared to the solution blending method, it uses no organic solvents, making it one of the most environmentally friendly methods. Therefore,

this method usually involves melting the organic material during the inorganic component mixing process. This method typically produces polymer-based hybrid materials by combining different inorganic materials, including silica, alumina, etc., with the polymers [72].

(c) Powder blending:

The powder blending method synthesizes organic-inorganic hybrid materials using solid-state powders. It is one of the most useful methods because it doesn't require a solvent or heating, unlike solution or molten blending. Moreover, it can be useful for organic materials with weak solubility, which organic solvents cannot treat, and highly melting materials, which inorganic materials cannot treat by melt-blending. Therefore, the most suitable approach is to employ the powder blending method in the synthesis of hybrid materials through high-energy ball milling [73]. This method mixes organic and inorganic materials through a series of energy transfers. Small particles break down agglomerates of inorganic materials, allowing them to mix homogeneously with the inorganic component of the polymer matrix. Depending on the organic-inorganic matrix interaction, the material that is formed in this way has the individual component properties as well as the new properties generated during the reaction.

1.13 Trimanganese tetroxide (Mn_3O_4)

Materials based on manganese oxide (Mn_3O_4) have received surprisingly significant scientific interest due to their technological applications such as ion exchange, molecular adsorption, water treatment, and catalysis [74]. The distinct morphology of Mn_3O_4 has significantly contributed to numerous applications in sensing, water treatment, and catalysts [75]. However, because of the multiple oxidation states of manganese oxide, the transformation into the formula (Mn^{+2} $(Mn^{+3})_2O_4$)

was made possible by redox processes, which included the coexistence of both Mn^{+2} and Mn^{+3} oxidation states, significantly contributing to absorption processes. Therefore, the Mn_3O_4 nanostructures exhibited a variety of intriguing properties, including strong catalytic activity, high carrier mobility, biocompatibility, good chemical and electrochemical stability, excellent thermodynamic stability, and environmental friendliness [76]. Hausmannite is considered one of the most stable Mn_3O_4 phases [77]. There are two Mn_3O_4 polymorph crystal structures: β-Mn_3O_4 (cubic, with a=b=c=8.7Å) and α-Mn_3O_4 (tetragonal, with a=b=8.14 Å and c=9.42 Å). Mn_3O_4 has a normal spinel structure in which Mn^{+2} ions are at the tetrahedral sites and Mn^{+3} ions are at the octahedral sites, which are arranged in a cubic close pack [75].

Figure (1.14), shows the detailed structure of different manganese sites in the hausmannite Mn_3O_4 unit cell. At room temperature, the crystal structure of Mn_3O_4 hausmannite is a spinel-distorted tetragonal structure [78]. It can crystallize in the BTC system to the crystal structure (space group I41/amd #141, $\alpha = \beta = \gamma = 90°$, with lattice constants of a = b = 5.762 Å and c = 9.470). The structure is deformed due to cell deformation caused by the Jahn-Teller effect [74]. The ionic manganese oxide formula is generally Mn_{+2} [Mn_2^{+3}] O_4 [79].

The spinal Mn_3O_4 structure's unit cell contains 32 oxygen atoms and 24 cations of divalent and trivalent manganese ions [80]. The Mn_3O_4 phase transformation depends mainly on the precursors used, as well as the calcination temperature and the molecular pressure effect of atmospheric air [81].

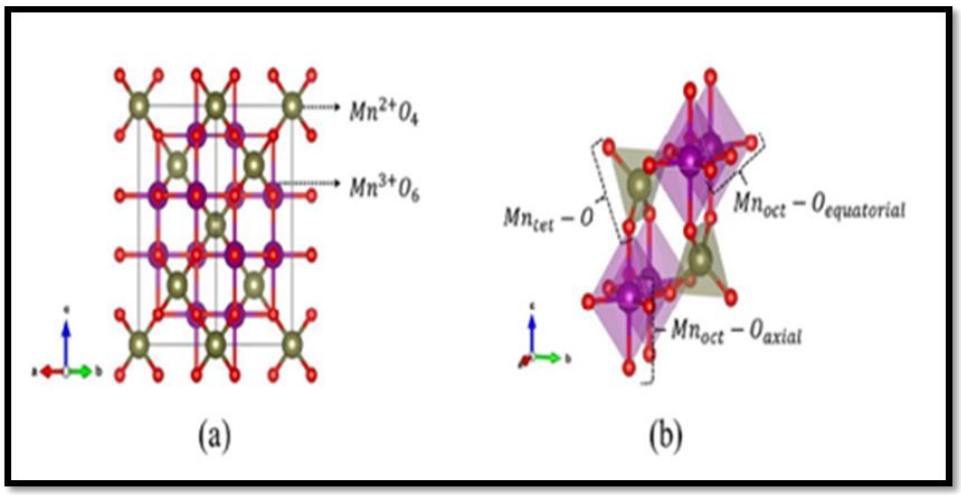

Figure 1.14: Hausmannite unit cell (a) Mn^{+2} ions in tetrahedral sites and Mn^{+3} ions in octahedral sites (b) Mn site's structure. [78]

Table 1.1: Some physicochemical characteristics of Mn_3O_4 [74].

Molecular Formula	Mn_3O_4
Molecular weight	228.812 g/mol
density	4.86 g/cm^3
Color	Brownish black
Melting point	1705°C
Boiling point	1564°C
Crystal structure	spinel
Crystal system	tetragonal
Lattice Parameters	a=b=5.757 Å, c=9.428 Å

1.14 Cobalt oxide (Co_3O_4)

In terms of the number of phases, cobalt oxide is one of the most diverse transition element oxides, with five different phases such as CoO, CoO_2, CoO (OH), Co_2O_3, and Co_3O_4 [82]. Cobalt oxide has received widespread attention for its many applications in chemical engineering and as an effective catalyst in environmental protection. Additionally, it is used as an anode in rechargeable lithium-ion batteries. In glass and ceramic processes, it serves as a pigment, and hydrocracking processes use it as a sensor and catalyst for raw fuel [83-85]. The general formula

for cobalt oxide's normal spinel structure is $A[B_2]\ O_4$. The Co^{+2} atoms occupy the A sites, which are tetrahedral, and the Co^{+3} atoms occupy the B sites, which are octahedral [86]. Eight combined forms of $A[B_2]\ O_4$ or $A_8B_{16}O_{32}$ make up the spinel unit cell [87]. Therefore, the Co_3O_4 unit cell consists of 56 ions [88]. as shown in Figure (1.15).

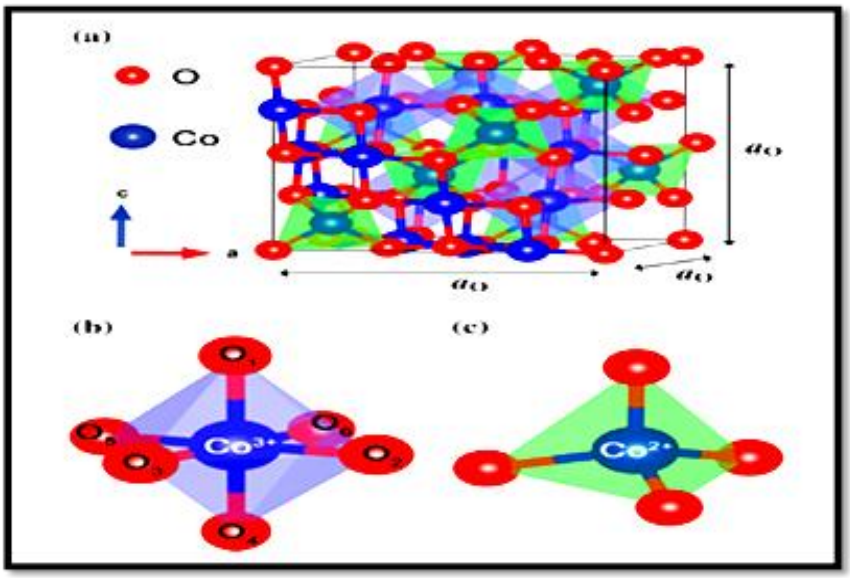

Figure 1.15: (a) Unit cell structure of Co_3O_4, (b) octahedral CoO_6 structure, (c) tetrahedral CoO_4 structure [89].

Cobalt oxide crystallizes in a spinel-cubic structure with two different oxidation states for cobalt, Co^{+2} and Co^{+3}. These states, in addition to oxygen ions, are located at the tetrahedral and octahedral interstitial sites, respectively, of the face-centered cubic lattice (FCC). In any case, the crystal fields that make up the tetrahedral and octahedral sites divide the five degenerate atomic d orbitals into two groups, and thus three d Co^{+2} electrons become unpaired, while the d Co^{+3} electrons are all paired, as shown in Figure (1.16) [90].

Cobalt oxide has a more complicated electronic structure than other transition metal oxides because it has two oxidation states, Co^{+2} and Co^{+3}, which cause different electronic configurations in the "d" orbital. However, all d-orbital electrons in Co^{+3} ions pair up in t_{2g} orbitals, and

each Co^{+2} ion consists of three single electrons in t_2 orbitals. However, the conduction bands of Co_3O_4 consist of the t_2 orbitals of Co^{+2} in addition to the t_{2g} orbitals of Co^{+3}. Therefore, the hybridization effect between the d orbitals in the two oxidation states of Co_3O_4 and the 2p orbitals of the oxygen anion will contribute to the formation of the valence band [91].

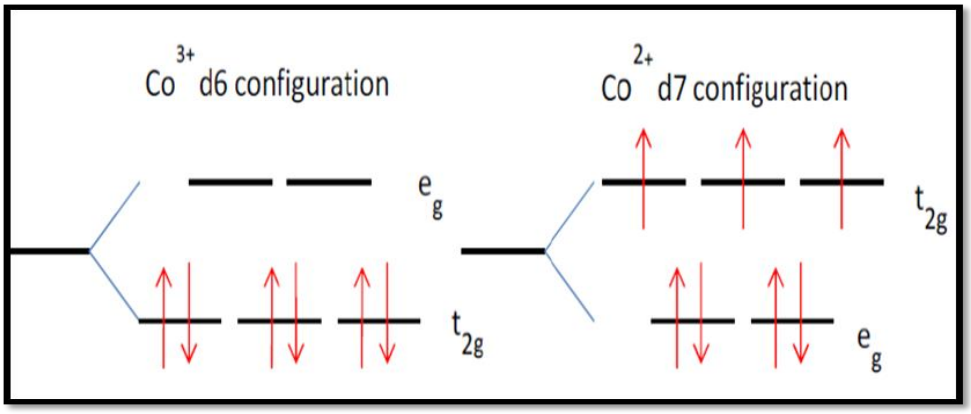

Figure 1.16: Crystal field splitting of the Co^{+3} ion in the octahedral field (left) and the Co^{+2} ion in the tetrahedral field (right). [87,90]

It is expected that six possible electronic transfers can occur due to the spinel formation of Co_3O_4, which can happen during the absorption of a photon that has an energy higher than the energy gap. Figure (1.17) demonstrated there are two possible pathways for charge transfer from the ligand to the metal. The first pathway involves the transfer of charges from O-2p to the two types of cobalt cations. The second path involves transferring charges from one metal to another, involving two distinct charge transfer processes between cobalt's two oxidation states: Co^{+2} and Co^{+3}. When the oxidation state in any lattice site of cobalt has changed, it can affect all LMCT and MMCT pathways. However, d-d excitations only change the local electronic structure and don't change the cobalt ion oxidation states [92]. Table (1.2), shows some of the physicochemical properties of Co_3O_4.

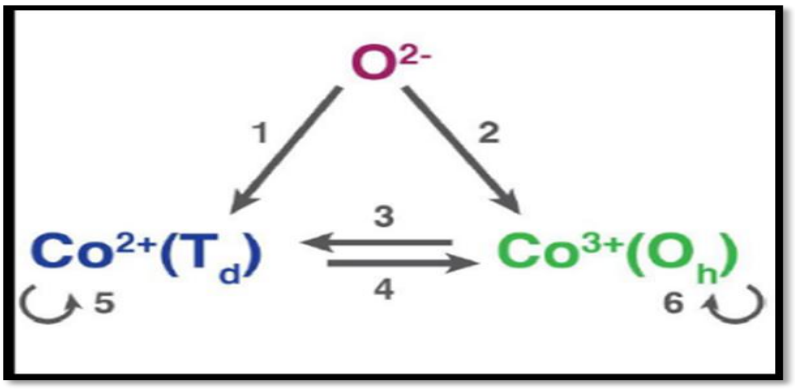

Figure 1.17: The six prospective optical excitation pathways in Co_3O_4 consist of oxygen anions and cobalt's two oxidation states. The Figure displays the two charge transfer pathways (1,2) from the ligand to the metal (LMCT), the two charge transfer pathways (3,4) from metal to metal (MMCT), and the d-d localize excitation pathways for a ligand field. [92]

Table 1.2: Some physicochemical properties of Co_3O_4 [93].

Molecular Formula	Co_3O_4
Molecular weight	240.8 g/mol
Color	black
Density	6.11 g/cm^3
Melting point	895 °C (1168 K)
Boiling point	900 °C (1173 K)
Crystal structure	Spinel
Crystal system	Cubic
Lattice Parameters	a=b=c= 8.05 Å

1.15 Magnetite (Fe_3O_4)

Magnetite, one of the most important magnetic materials, has gained significant attention due to its distinctive properties, which have opened up many applications such as sensors, batteries, catalysts, and the delivery of targeted drugs and catalysts [94]. Iron oxides are considered one of the most important groups of transition metal oxides. Although the ionic bond is dominant, they show a covalent bond between cations and anions [95]. Magnetite is considered the most stable structure among the iron oxide phases according to the formation temperature [96]. When magnetite is at room temperature, it forms crystals in a spinal-reversed

shape with the space group Fd3m and the lattice parameter a = 8.397 Å [97]. The magnetite unit cell specifically packs O^{-2} ions into a distorted, face-centered cubic lattice. Fe^{+3} ions occupy the A-site and surround it with oxygen ions to form a tetrahedron, while an equal number of Fe^{+2} and Fe^{+3} ions occupy the B-site and surround it with oxygen ions to form an octahedron [98]. In general, the magnetite formula is $[Fe^{+3}]$ $A[Fe^{+2}Fe^{+3}]BO_4$ [95]. The magnetite unit cell at room temperature is as shown in Figure (1.18a) [99].

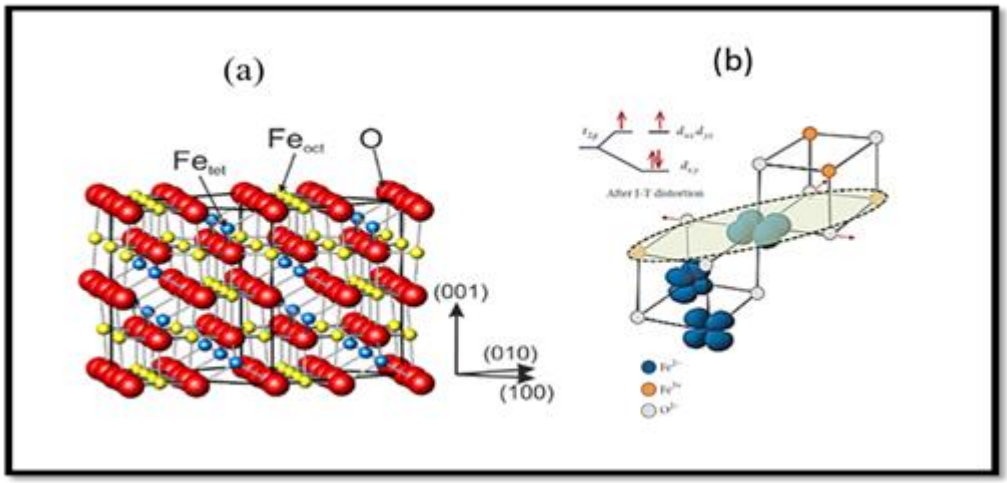

Figure 1.18: (a) magnetite unit cell, (b) The energy separation of the Jahn-Teller distortion and the concept of trimeron in a single $Fe^{+2}O_6$ octahedron [97,99].

Fe^{+2} and Fe^{+3} ions bound at the tetrahedral and octahedral sites strongly affect the electrical properties of magnetite. This explains the reason for the excellent conductivity of magnetite compared to other oxides such as Fe_2O_3 and FeO [100]. At room temperature, magnetite is believed to conduct electricity because electrons jump between the Fe^{+2} and Fe^{+3} ions ($Fe^{+2} \leftrightharpoons Fe^{+3} + e^-$) in the octahedral site (B). The extra electron in Fe^{+2} occupies only the minority band t_{2g}, which is located near the Fermi level and which explains the magnetite conductivity as a semi-metal as energy band calculations show [101, 102]. As shown in Figure (1.18b) [97]. In addition to the magnetite structural features, the material displays other

properties, including the Curie temperature, observed at 860 K. The Verwey transition at 120 K explains the high rotational polarization (100%), as well as the transition from the inverse spinal cubic structure to the monoclinic structure [103]. The formula AB_2O_4 for magnetite shows that the inverse spinal structure is the opposite of the normal spinal structure. Because there is no crystal stabilization field, the inverse spinal structure places the Fe^{+2} ions in octahedral sites B instead of tetrahedral sites A. It also spreads the Fe^{+3} ions evenly between sites A and B. The field distributes the Fe^{+2} ions between sites A and B to stabilize it at one of the two sites, with sufficient crystal stabilization energy at the B sites [104]. Table (1.3), shows some physicochemical properties of magnetite.

Table 1.3: Some physicochemical characteristics of magnetite [105].

Molecular Formula	Fe_3O_4
Molecular weight	231.533 g/mol
Color	black
Density	5.18 g/cm^3
Melting point	1583-1597 °C
Boiling point	2,623°C
Crystal structure	inverse spinel
Crystal system	cubic
Lattice Parameters	a=b=c=8.396 Å

1.16 Thin film concept

To describe the atoms of matter arranged in a single layer or several successive layers whose thickness does not exceed 1 micron, they are called thin films. Thin film preparation technology, one of the most advanced modern technologies, has significantly contributed to the study of semiconductor and metal development by providing a clear picture of new physical and chemical properties. According to the nature of thin

films formed in two dimensions, their properties generally differ from those of bulk materials. This is because in a three-dimensional bulk material, particles are subject to forces from all directions, whereas in a thin film, these forces only affect the particles located at the surface. In 1852, Bunsen & Grove prepared thin films for the first time using the chemical reaction technique in the middle of the nineteenth century. Faraday followed them several years later, in 1857, using the thermal evaporation technique to prepare a thin metal layer [106]. In 1947, H. A. McMaster and W. O. Lytle registered an American patent for the preparation of commercially thin films through spray pyrolysis, which involved the deposition of conductive metal oxides on heated glass substrates [107, 108]. Typically, scientists deposit the film layer on specific plates that align with the scientific requirements and nature of the proposed study. These plates can be in several forms, including glass, quartz, and aluminum slides, as well as silicon wafers [109]. Thin films are of significant technological and industrial importance, especially in optical and electronic applications. Thin film applications have gained significant importance over the decades due to their use in capacitors, electrical resistors, transistors, and integrated circuits in digital devices, among other things. Many modern technologies, particularly in the optical fields, utilize thin films in the production of thermal, high-reflection, and regular mirrors, as well as semi-transparent, reflective coatings for solar cells, non-absorbent mirrors, filters, and materials for optical phenomenon interference [108].

1.17 Thin films deposition techniques

Essentially, thin film deposition techniques are divided into two main groups: physical and chemical techniques [110,111], which are as shown in Figure (1.19).

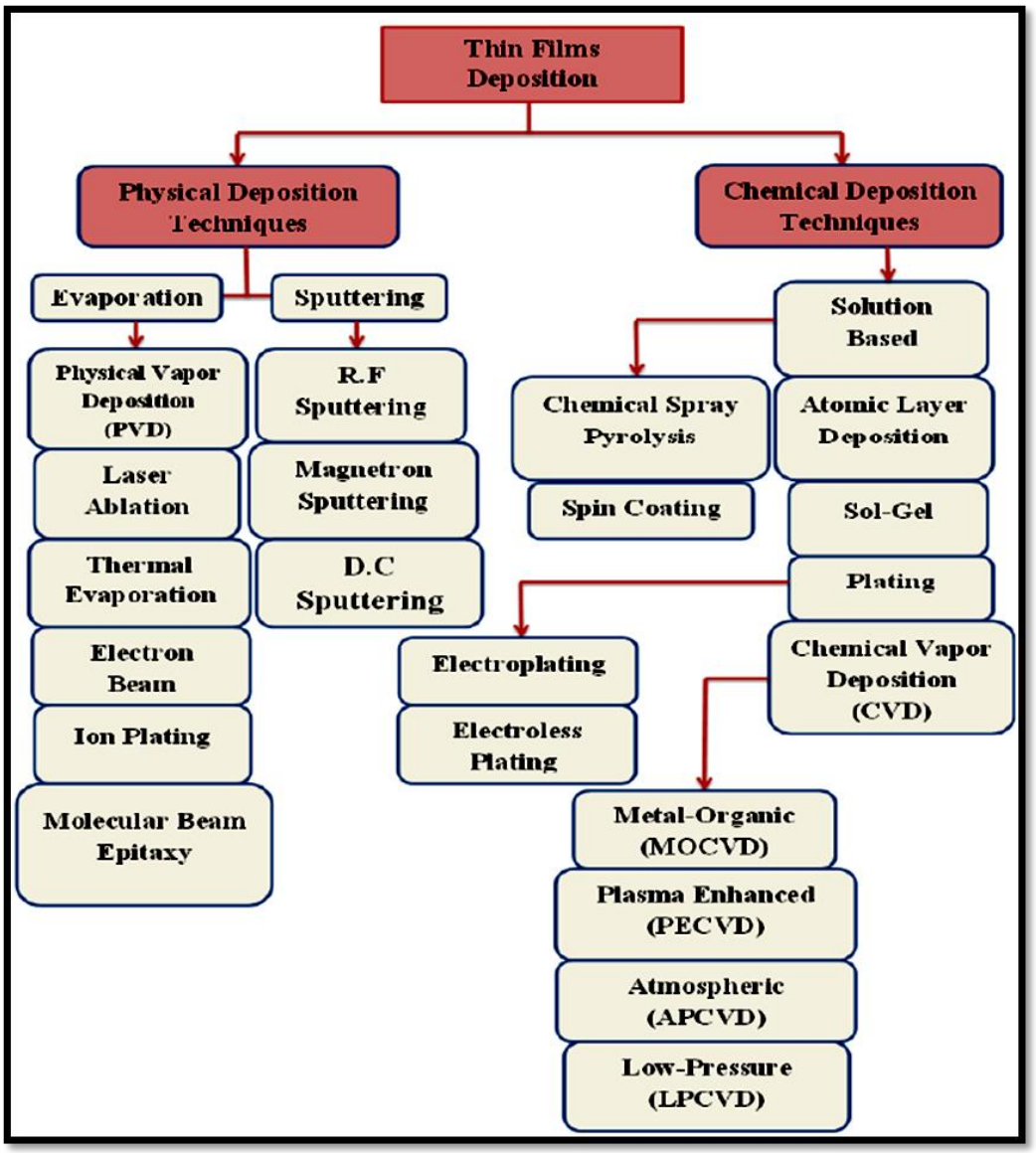

Figure 1.19: Classification of chemical and physical techniques for thin film deposition [111].

1.17.1 Spin coating technique

Spin coating, a widely used chemical deposition technique, has been instrumental in the development of sensors for both organic and inorganic materials. Through this technique, it became possible to deposit highly reproducible and homogeneous films. The principle of spin coating is based on the solution adhesion force at the substrate interface, as well as the centrifugal force generated by the high-speed during

rotation. As a result, these two forces will generate strong shear at the interface, resulting in the formation of a thin layer of solution with a controlled thickness based on solution concentration, angular velocity, and viscosity [112]. There are many important factors that affect the film's uniformity, such as solution concentration, liquid viscosity, angular velocity, spin time, and solvent evaporation rate.

1.18 Literatures review

Jokar *et al*. (2014) used the chemical precipitation method to synthesis Fe_3O_4 magnetic nanoparticles. They then used the in-situ doping polymerization method with hydrochloric acid to create PAni-Fe_3O_4 nanocomposites. The magnetic PAni-Fe_3O_4 nanocomposites were characterized using XRD and SEM techniques. They also used the vibrating sample magnetometer (VSM) technique to study the magnetization properties of the magnetic nanocomposite at RT. Electrical conductivity and magnetic tests of the prepared magnetic nanocomposite showed that it has good conductivity and effective magnetic behavior. The batch adsorption mode demonstrated the adsorbent's ability to remove fluoride from water. The results showed that the adsorbent has great efficacy against fluoride, and that the adsorption that occurs is fast and depends on the adsorbent dose and pH [113].

Shambharkar *et al*. (2014) synthesized PAni-Mn_3O_4 nanocomposites using the in situ chemical oxidation method for aniline monomers. They used different concentrations of aniline and Mn_3O_4 (3.3:1 and 2.5:1) and used ammonium persulfate as an oxidizing agent in an aqueous solution of sodium dodecylbenzene sulfonic acid as a surfactant, all under N_2 atmosphere and at a temperature of 5 °C. They used XRD and FT-IR to characterize the crystalline phase and structural components of Mn_3O_4 NPs and PAni-Mn_3O_4 nanocomposites. The results of FT-IR

spectroscopy and TGA revealed that the interaction between Mn_3O_4 NPs and the PAni matrix can improve thermal stability. PAni and PAni-Mn_3O_4 nanocomposites at concentrations (3.3:1) and (2.5:1) showed electrical conductivities of 3.26×10^{-4}, 8.11×10^{-7}, and 3.93×10^{-7} S/cm, respectively. They proved that the conductivity decreases as the Mn_3O_4 content in the PAni matrix increases. They also proved through magnetic tests that the coercive force (H_c) and residual magnetism (M_r) increase with increasing Mn_3O_4 content in the PAni matrix at a temperature of 5 °C [114].

Xu et al. (2015) synthesized Co_3O_4 NPs using the carbon assisted method, degreasing cotton as a template, and prepared the core-shell Co_3O_4-PAni nanocomposite structure using the in-situ polymerization method. They characterized the prepared samples using XRD, TEM, FT-IR, and XPS techniques. The test results showed that amorphous PAni completely covered the Co_3O_4 spinel surface. Particles approximately 100 nanometers in size formed the Co_3O_4-PAni nanocomposite core-shell structure. The interfacial interaction between the components of the nanocomposite's shell-core structure significantly enhanced the microwave absorption properties. The researchers' findings indicated that the maximum loss in reflection in PAni Co_3O_4 at a thickness of 2.5 mm was more than -45.8 dB at 11.7 kHz. When the thickness was between 2 and 5.5 mm, the absorption band width, in addition to the reflection loss, was less than -10 dB, reaching 14.1 kHz and ranging from 3.9 to 18 kHz. They concluded that the simple and low-cost synthesis of Co_3O_4-PAni nanocomposite could make it a promising nanomaterial with high efficiency in absorbing microwaves [115].

Hai et al. (2016) synthesized the PANI-Co_3O_4 nanocomposite core-shell structure by using a carbon-assisted method and in situ polymerization for use in supercapacitor applications. They investigated factors affecting the

performance of supercapacitors using XRD, UV-Vis spectrophotometry, SEM, TEM, and water contact angle (WCA). The shell-core structure of the PAni-Co_3O_4 nanocomposite synthesis, which is made up of amorphous polyaniline, had many benefits, including a large surface area, a small energy band gap, and hydrophilicity. These properties were the main reason why the electrochemical nanocomposite worked so well as supercapacitor electrode materials. They performed the cyclic voltammetry (CV) measurements, electrochemical impedance spectroscopy (EIS), and galvanic charge/discharge measurements in an aqueous solution with a concentration of 6 M KOH. The core-shell structure of the PAni-Co_3O_4 nanocomposite had a high specific capacitance of 1184 F g^{-1} at 1.25 A g^{-1}. It was also very stable, keeping 84.9% of its capacitance after 1000 cycles of galvanostatic charge and discharge. It has excellent conductivity and ion diffusion behavior, according to the results [116].

Sen et al. (2016) studied gaseous sensitivity to carbon monoxide (CO) through nanocomposites prepared from PAni-Co_3O_4 nanocomposites at RT. The researchers prepared Co_3O_4 NPs using the traditional chemical precipitation method and incorporated them into the PAni matrix using ultrasonication. They characterized the prepared nanoparticles using a variety of techniques, including FT-IR spectroscopy, UV-Vis spectroscopy, X-ray diffraction, and morphological examinations using the FE-SEM technique. At RT, the PAni-Co_3O_4 nanocomposites sensors showed distinct selectivity for CO gas. The prepared devices recorded a remarkable high responsivity of 0.81 at 75 ppm concentration of CO gas, with a 40-second response time. They also studied the effect of humidity on the PAni-Co_3O_4 nanocomposite sensor responsivity, in addition to its gas sensitivity [117].

Singh et al. (2016) used cetyltrimethylammonium bromide to synthesize Mn_3O_4 spherical nanoparticles. They later modified the Mn_3O_4 spherical nanoparticles in the presence of glutaraldehyde and polyvinyl sulphonic acid with polyaniline, preparing an electrochemical biosensor based on polyaniline nanofibers- Mn_3O_4 through an in-situ polymerization process. This biosensor detects bisphenol A (BPA), an endocrine disrupting chemical. The researchers used X-ray diffraction, FT-IR spectroscopy, and SEM to characterize the tyrosinase (Tyrs) molecules covalently immobilized to the surface of modified PAni-modified Mn_3O_4 nanofibers. In the concentration range of 0.004–0.09 × 10^{-6} mol L^{-1} and 0.2–0.8 × 10^{-6} mol L^{-1}, the electrochemical biosensor recorded a sensitivity of 0.776 $mAmM^{-1}Lcm^{-2}$ and 0.134 $mAmM^{-1}Lcm^{-2}$, respectively, with a response time of 20 s [118].

Li et al. (2017) used a modified co-precipitation method to synthesis Fe_3O_4 NPs. Next, they used the in-situ polymerization method to deposit the conductive polymers, polypyrrole and polyaniline, on the surface of Fe_3O_4 NPs in the Fe_3O_4/PPy/PANI ternary nanocomposite preparation. The strong attraction between the carbonyl group of polypyrrole and the conjugated chains of polyaniline made it possible to connect polypyrrole to polyaniline. The prepared ternary nanocomposites showed absorption properties towards microwaves, as the results showed an absorption band of 10.7 GHz (6.7–17.4 GHz). The results also showed that the maximum reflection loss at GHz is -40.2 dB. They also concluded that the process of combining Fe_3O_4 NPs with two conductive polymers has potential for application in microwave-absorbing materials [119].

Sharma et al. (2017) used a simplified reduction method to synthesize PAni-Mn_3O_4 nanocomposite in one step, doping Mn_3O_4 NPs with PAni matrix at different concentrations (1 mM and 3 mM). Then they proceeded to characterize the optical and morphological properties, as

well as conduct thermal and electrical examinations. The polymeric matrix doped the Mn_3O_4 nanoparticles, as revealed by FT-IR and UV-Vis spectroscopy. The SEM micrographs also demonstrated the agglomeration of polyaniline particles and the formation of fiber-like structures in the nanocomposites with multiple holes. The PAni nanocomposites sensor, when exposed to acetone, benzaldehyde, and ethanol vapors at a 3 mM concentration, exhibited a notable sensing response and 1.5 sensitivity for acetone vapor. This improvement in controllable properties at the interface stems from molecular and supramolecular interactions. They also concluded that the synthesized nanocomposite could be an effective potential sensor for acetone in terms of response and recovery [120].

Kashyap et al. (2019) synthesized polyaniline nanofibers using the in situ oxidative polymerization method with aniline monomers and deposited them on silicon substrates to develop a gas sensor for toluene. They used XRD, FE-SEM, HR-TEM, and FT-IR examinations to confirm the PAni NFs. HR-TEM and FE-SEM examinations revealed the PAni NFs structure, revealing diameters ranging from 70-80 nm and lengths of 400-450 nm. PAni NFs have detected volatile organic compounds (VOCs) such as ethanol, toluene, acetone, and chloroform at concentrations ranging from 50 ppm to 1000 ppm. The gas sensor based on PAni NFs showed specific selectivity for toluene at low concentrations compared to other VOCs. The sensor also showed a sensitivity to toluene gas of 24.5% at a concentration of 50 ppm. The sensor also revealed a toluene response time of 92 s and 120 s, respectively, at a concentration of 400 ppm. Finlay, they concluded that the prepared gas sensor showed stability in operation over a period of 45 days [121].

Venkatreddy et al. (2020) used the in-situ polymerization method to prepare PAni-Co_3O_4 nanocomposites using cobalt nitrate as a metal

precursor, polyaniline as a polymerization agent, and aloe vera (A.V.) gel as a fuel. They characterized the prepared nanocomposites using XRD, SEM, and TEM techniques. The PAni-Co_3O_4 nanocomposites had better electrical properties than the PANI and Co_3O_4 nanoparticles alone. This is because Co_3O_4 and PAni interact with each other at the interface. At different temperatures, tests showed that the D.C. electrical conductivity increases with the increase in the Co_3O_4 concentration from 10 to 50% in the nanocomposite, which indicates the possibility of using it in solar cell applications, optical devices, and LED devices [122].

Payami et al. (2020) synthesized the modified graphene oxide (GO) using a click reaction, assisted by the novel alkyne-terminated ferrocene. They also used physical mixing to prepare a ternary nanocomposite of PAni, Mn_3O_4 NPs, and GO (GO-Fc) for use in batteries as a supercapacitor. They also used the FT-IR, proton nuclear magnetic resonance (^{1}H NMR), and carbon nuclear magnetic resonance (^{13}C NMR) to describe the new alkyne-terminated Fc compound structure. To study the structure and morphology of newly synthesized materials and to test their electrochemical performance, they used tools such as cyclic voltammetry (CV), galvanostatic charge-discharge (GCD) measurement, FT-IR, FE-SEM, XRD, EDX, and electrochemical impedance spectroscopy (EIS). The GO-Fc/Mn_3O_4/PANI nanocomposite showed a capacity retention capacity of up to 80% as well as a high charge storage capacity of 233 mAh g^{-1} at 2.5 A g^{-1}. The symmetrical electrode system produced a high-power density of 42.6 Wh kg and 5.56 kW kg. The researchers concluded that GO-Fc/Mn_3O_4/PANI nanocomposite is a candidate composite [123].

Fan et al. (2021) used the hydrothermal method as well as in situ polymerization to prepare a novel PAni-Co_3O_4 supercapacitor electrode deposited on a foamed nickel base. Through structural and morphological

examinations using XRD, SEM, TEM, and XPS, they demonstrated that the cobalt oxide took the form of rods, uniformly coated with PAni. Then they conducted an electrochemical study and found that the PANI-Co_3O_4 composite specific capacity at $1Ag^{-1}$ increased by 14.7 times compared to the values recorded for Co_3O_4 alone, reaching 3105.46 Fg^{-1} (31.05 F cm^{-2}). The study also showed that the electrical power after 3000 cycles maintained 74.81% of its original value, which indicates cycle stability. The AC properties of the PAni-Co_3O_4 composite also demonstrated an energy density of 58.84 W h kg^{-1} at 0.16 kW kg^{-1}. However, they concluded that the study indicates not only a new method for preparing metal oxide semiconductors with PAni but also great potential applications in high-performance energy storage devices [124].

Nate et al. (2021) prepared PAni-Co_3O_4 nanofibers using both the oxidation precipitation and interfacial polymerization methods. The researchers investigated the synthesis materials using FT-IR, UV-Vis, SEM, TEM, XRD, and EDX techniques. They simultaneously demonstrated the formation of PAni NFs through morphological examination and confirmed the presence of Co_3O_4 NPs in the PAni nanocomposite using XRD and EDX. They also used cyclic voltammetry (CV) and pulsed differential voltammetry (DPV) for simultaneous primaquine and proguanil electrochemical detection. To accomplish this, they modified a vitrified carbon electrode with PAni NFs and Co_3O_4 NPs (PAni-Co_3O_4/GCE). Moreover, they found that the ideal pH for the sensor response was 3.5 for both drugs. Primaquine and proguanil, respectively, yielded a LOD of 2.07 nM and 1.42 nM, both within the linear range of 0.020–0.036 and 0.016–0.028 mM. Furthermore, they investigated the practical application of PAni-Co_3O_4/GCE in human urine using a variety of interfering agents. They recovered an amount between 94 and 105% through the application, leading them to conclude that the

PAni-Co_3O_4 nanocomposite could be used in quality control processes through the manufacture of electrochemical sensing devices [125].

Al-Gharram et al. (2021) used electrochemical polymerization to deposit PAni-CSA/ (Co_3O_4 NPs) nanocomposite films at different weight percentages (1, 3, 6, and 12%) of Co_3O_4 NPs on ITO-glass substrates. Then they studied the structural properties of PAni nanocomposites films with Co_3O_4 using SEM and XRD techniques. They also used UV spectra to determine and study the optical properties of the nanocomposite films. It was observed that when Co_3O_4 was added to the nanocomposite film, the optical energy gaps at the transitions π-π* and π-polaron got smaller. The optical properties revealed potential applications for the prepared nanocomposite films in modern electromagnetic and optical devices [126].

Lee et al. (2023) synthesized a new ternary nanohybrid composite out of PAni, Co_3O_4, and TiO_2 to sense acetone at 25 °C. For this purpose, they combined individual Co_3O_4 and TiO_2 nanoparticles synthesized by the sol-gel method with polyaniline NPs during the polymerization synthesis method. The target gas sensing properties of nanocomposite sensors, which were prepared from Co_3O_4-TiO_2, PAni-TiO_2, and PAni-Co_3O_4-TiO_2, were systematically evaluated at 25 °C and without UV illumination. The sensing results revealed that we prepared the ternary nanocomposite with weight concentrations of 0.01 wt.% PAni, 0.85 wt.% TiO_2, and 0.15 wt.%. Co_3O_4 has a high responsivity to acetone at 25 °C under UV illumination. Therefore, they concluded that the gas sensor's better performance is due to the p-n heterojunctions, polyaniline effects, and UV radiation [127].

Kroutil et al. (2023) used different types of polyanilines as active layers in sensor design because of their ease of setup and low cost. Polyaniline films show high sensitivity to gas concentrations at room temperature.

The developed sensor operates based on the concept of chemoresistance, a phenomenon where resistance shifts in response to changes in gas concentrations. They prepared the polyaniline active layers using three different polymerization solutions: sulphuric acid solution, acetic acid solution, and water solution. The evaluation of the active layers in a controlled environment involved testing their ability to detect carbon monoxide, ammonia, nitrogen monoxide, acetone, and relative humidity in synthetic air. However, they concluded that the polymerized layers in acetic acid showed a very high sensitivity to ammonia gas [128].

Shaker et al. (2024) used the in-liquid laser ablation technique to synthesis colloidal polyaniline nanoparticles. SEM, X-ray diffraction, and UV-Vis absorption techniques were used to examine the structural, morphological, and optical properties of the synthesized nanoparticles. The structural XRD examinations revealed that the PAni NPs have a semi-crystalline structure with (121) crystalline orientation. Morphological analysis showed that the PAni NPs are platelet-shaped with a 40 nm average size. The PAni optical energy bandgap is 3.75 eV, according to the optical properties. The prepared PAni/Si heterojunction photodetector demonstrated rectifying properties and a 3.4 ideality factor. At 610 nm, the maximum PAni/Si heterojunction photodetector responsivity was 0.58 A. W^{-1}. At a bias voltage of 8.5 volts, the photodetector device showed 80% sensitivity at the 9.7 mW/cm^2 light intensity. The PAni/Si heterojunction's external quantum efficiency and detectivity values at 610 nm were calculated to be 2.9×10^{11} Jones and 1.17×10^2 %, respectively [129].

Jarad (2024) prepared a p-n PAni/Si heterojunction with a 300-nm thickness using the spin coating method. This involved depositing PAni films on the top surface of the silicon wafer, followed by thermal evaporation to deposit silver and aluminum electrodes on the top and

bottom surfaces, respectively. The electrical characteristic results demonstrated the repeatability of the prepared p-n PAni/Si, which had a very high correction factor. Results from spectroscopy and photoresponse analysis confirm the potential of the PAni/Si heterojunction as a broadband photodetector. Moreover, the prepared photodetector showed almost high sensitivity (≈200%) in the UV region at 2.0 - 3.5 eV, as compared to other commercial optical photodetectors, such as the OPT detector [130].

Wang et al. (2024) utilized both the drop casting method and the aerosol inkjet printing method to create a gas sensor based on polyaniline. They examined their sensitivity to ammonia gas, finding that the aerosol inkjet printing gas sensor exhibited a shorter response time and recovery time than the drop casting gas sensor. They also documented morphological observations to enhance the sensing mechanism of the prepared gas sensors. However, they confirmed that the aerosol printing method, which transfers the polyaniline crystalline structure to the sensor during its preparation, significantly impacts the sensor's ultra-fast response and recovery [131].

Darvina et al. (2024) synthesized Fe_3O_4 NPs by magnetic separation and ball milling iron sand, then integrated them into the PAni gelation process at varying concentrations (30%, 40%, 50%, 60%, and 70%) through spin coating, resulting in the deposition of Fe_3O_4 -PAni nanocomposites on glass substrates. They used XRD, SEM, VSM, as well as A.C. electrical measurements with an LCR meter to demonstrate a relationship between the concentrations and the crystallite size. The crystal size decreased as the concentrations rose from 30% to 40%, then increased at 50%, and then decreased again at 60% to 70%. FT-IR spectroscopy confirmed the chemical bonding between Fe_3O_4 NPs and PAni. The thickness variation

of the nanocomposite films with the Fe_3O_4 concentrations was confirmed by FE-SEM cross-section images, which revealed thicknesses of 16.54 m, 17.82 m, 19.36 m, and 24.4 m, respectively. Electrical property tests indicated different resistance values at 7.36 mΩ, 8.388 mΩ, 8.101 mΩ, 8.53 mΩ, and 3.53 mΩ for the Fe_3O_4 concentrations corresponding to the measured capacitance. The structural and electrical properties of Fe_3O_4/PAni nanocomposites indicate the possibility of using them in a variety of different applications [132].

Elashmawi et al. (2024) synthesized pure polyaniline and pure magnetite (Fe_3O_4) to prepare and characterize PAni-Fe_3O_4 nanocomposites. The FT-IR examination of the nanocomposite demonstrated the successful polymerization of polyaniline on Fe_3O_4 NPs. The optical examination of the nanocomposites revealed wide absorption bands that corresponded to different functional groups at specific wavelengths. The blue shift in the absorption peaks indicates a hydrogen bonding interaction between the oxygen and nitrogen atoms on the Fe_3O_4 NPs. The nanocomposites exhibited a robust interaction between PAni and Fe_3O_4, as evidenced by the weakening of Fe-O bonds due to a decrease in absorption intensity as the wave number of Fe_3O_4 NPs decreased. Morphological examinations revealed that Fe_3O_4 NPs have a regular sphere shape with an average 16 nm diameter and an irregular distribution due to agglomeration in secondary particles caused by attractive forces. PAni-Fe_3O_4 nanocomposites with a core/shell structure are made when the Fe_3O_4 nanoparticles change shape and are coated with PAni. The electron diffraction technique confirmed the crystalline structure of the Fe_3O_4 NPs through the compatibility of the diffraction rings with magnetite. The researchers explained that the PAni nanocomposites magnetic properties result from the magnetic property transfer by the incorporation of

nanoparticles. Magnetic saturation measurements showed that increasing the Fe_3O_4 concentration leads to an improvement in magnetization. However, they came to the conclusion that doping changes the magnetic behavior of nanocomposites and is an important way to control the magnetization process. This makes it easier to use these materials for possible purposes, like magnetic sensors and data storage [133].

1.19 Objective of the study:

1. Synthesize polyaniline nanofibers (PAni NFs), magnetite nanoparticles (Fe_3O_4 NPs), tetramanganese oxide nanoparticles (Mn_3O_4 NPs), and cobalt oxide nanoparticles (Co_3O_4 NPs).
2. Preparation of PAni NFs, Mn_3O_4 NPs, Co_3O_4 NPs, and Fe_3O_4 NPs films, as well as PAni-MO nanocomposites prepared with different volumetric ratios of PAni and metal oxide (MO) nanoparticles.
3. Characterization the structural, morphological, optical, and electrical properties of all prepared samples.
4. Application of the PAni NFs and Mn_3O_4, Co_3O_4, and Fe_3O_4 nanoparticle films, as well as PAni-MO nanocomposite films for gas sensing and photodetection.

الخلاصة

في هذه الدراسة، حضرت ألياف البولي أنيلين النانوية وجسيمات اوكسيد الحديد النانوية (المغنتايت) باستعمال التقنية الحرارية المائية، في حين استعمال عملية الترسيب الكيميائي في تحضير جسيمات رباعي اوكسيد المنغنيز النانوية والجسيمات النانوية لأوكسيد الكوبالت. تم تهيئة لاغشية المرسبة على قواعد زجاجية وسيلكونية للألياف النانوية للبولي أنيلين وأوكسيدات المعادن المتضمنة كل من أوكسيد أوكسيد المنغنيز وأوكسيد الكوبالت والمغنتايت وأغشية المتراكبات النانوية للبولي أنيلين مع كل واحد من أوكسيدات المعادن عند نسب حجمية مختلفة باستعمال عملية الطلاء الدوراني.

أكدت فحوصات حيود الأشعة السينية الطبيعة البلورية لأغشية البولي أنيلين والتراكيب متعددة التبلور لأغشية اوكسيدات المعادن بأطوار: رباعي السطوح Hausmannite للجسيمات النانوية لأوكسيد المنغنيز ومغزلي مكعب متمركز الأوجه لأوكسيد الكوبالت، فضلا عن الطور المغزلي المعكوس المكعب للمغنتايت.

أظهرت فحوصات المجهر الالكتروني الماسح عن تراكيب تشبه الألياف بأقطار نانوية تتراوح بين ٤٦ و٨١ نانومتر للبولي انيلين، ومجموعة من الجسيمات النانوية الكروية لأوكسيد المنغنيز وأوكسيد الكوبالت والمغنتايت بأقطار تتراوح بين ٣٤ و٥٣ نانومتر وبين ٢٠ و٢٦ نانومتر وبين ٥٨ و٨٦ نانومتر على التوالي. كما أظهرت الفحوصات أشكال تشبه الألياف مغطاة بالجسيمات النانوية لاوكسيدات المعادن للمتراكبات النانوية للبولي أنيلين بأقطار (٣٣-٥٣) نانومتر للمتراكبات النانوية للبولي أنيلين مع رباعي أوكسيد المنغنيز و(٣٣-٤٦) نانومتر للمتراكبات النانوية مع أوكسيد الكوبالت و (٢٧-٤٦) نانومتر للمتراكبات النانوية مع المغنتايت.

كشف طيف الأشعة فوق البنفسجية والمرئية للألياف النانوية للبولي أنيلين عن ذروتي امتصاص عند ٢٩٦ نانومتر و٦٢٧ نانومتر، تعود الى الأنتقالات الإلكترونية (π-π^*) في حلقة البنزينويد والانتقالات الإلكترونية من حلقة البنزينويد إلى حلقة الكينويد، وقد أزيحت تلك الذروات نحو الأطوال الموجية الطويلة في المتراكبات النانوية للبولي أنيلين مع أوكسيدات المعادن مما يؤكد نقص في فجوة الطاقة للمتراكبات النانوية للبولي أنيلين مع أوكسيدات المعادن.

طيف الأشعة تحت الحمراء أظهر مجموعة من ذروات الأمتصاص تعود للمجاميع الوظيفية الفعالة التي تشير الى تشكل الألياف النانوية للبولي أنيلين، وقد أزيحت مواضع تلك

الذروات نحو اللون الأحمر في أطياف المتراكبات النانوية للبولي أنيلين مع أوكسيدات المعادن مما يشير الى التفاعل القوي بين البولي أنيلين مع أوكسيدات المعادن.

أظهرت توصيلية التيار المستمر (D.C.) لأغشية للبولي أنيلين وأوكسيدات المعادن والمتراكبات النانوية للبولي أنيلين مع أوكسيدات المعادن عن زيادة في التوصيلية المستمرة مع زيادة درجة الحرارة مما يؤكد سلوك شبه الموصل للأغشية المحضرة. كذلك بينت حسابات طاقة التنشيط عن نقص في قيمة طاقة التنشيط مع زيادة محتوى أوكسيد المعدن في المتراكبات النانوية للبولي أنيلين مما يشير الى زيادة التوصيلية المستمرة.

فحوصات توصيلية التيار المتردد (A.C.) لأغشية البولي أنيلين ومتراكباتها النانوية مع أوكسيدات المعادن أظهرت زيادة في توصيلية التيار المتردد مع زيادة التردد من ٥٠ هرتز إلى ٣ ميجاهرتز، ومع زيادة محتوى أوكسيد المعدن في متراكبات البولي أنيلين النانوية.

أظهرت الخصائص العزلية لأغشية البولي أنيلين ومتراكباتها النانوية مع أوكسيدات المعادن نقص في ثابت العزل الكهربائي وعامل الفقد مع زيادة التردد لأغشية البولي أنيلين وأوكسيدات المعادن ومتراكباتهما النانوية، وزيادة كل من ثابت العزل وعامل الفقد مع زيادة محتوى أوكسيد المعدن في المتراكبات النانوية للبولي أنيلين.

قياسات تأثير هول أثبتت سلوك شبه الموصل من النوع p للبولي أنيلين وأوكسيد الكوبالت ومتراكباتهما النانوية، في حين أظهرت سلوك شبه الموصل من النوع n لرباعي أوكسيد المنغنيز والمغنتايت ومتراكباتهما النانوية مع البولي انيلين.

أظهرت خصائص سعة – فولتية (C-V) كدالة لجهد الأنحياز العكسي نقص في السعة مع زيادة جهد الأنحياز العكسي لأجهزة المفارق الهجينة للبولي أنيلين وأوكسيدات المعادن ومتراكباتهم النانوية، ونقصها مع زيادة محتوى أوكسيد المعدن في أغشية المتراكبات النانوية. من خلال ميل الجزء الخطي لمخطط (C^{-2} – V) أظهرت النتائج تكون المفرق الهجيني الحاد بين أغشية البولي أنيلين وأوكسيدات المعادن ومتراكباتهم النانوية مع القواعد السيلكونية من النوع n و p. فضلا عن نقص في قيمة جهد البناء الداخلي (V_b) مع زيادة في محتوى أوكسيد المعدن في مصفوفة البولي أنيلين.

أظهرت خصائص الأستجابة الضوئية لأجهزة المفارق الهجينة للبولي أنيلين وأوكسيدات المعادن ومتراكباتهم النانوية من خلال منحنيات تيار- فولتية (I-V) في الظروف

المظلمة والمضيئة، ولوحظ أن التيار الضوئي قد أزداد مع زيادة شدة الضوء ومع زيادة تركيز أوكسيد المعدن في مصفوفة البولي أنيلين وهذا يدعم سلوك الثنائي الضوئي. كما أظهرت قيم عامل المثالية العالية السلوك غير المثالي للثنائيات الضوئية المحضرة.

أظهر منحنى التيار الضوئي مع الزمن (I-t) لكل نبضة تشغيل / إيقاف لأجهزة المفارق الهجينة التي أجريت تحت أطوال موجية مختلفة (٣٠٠-٥٠٠ نانومتر)، زيادة في التيار الضوئي مع كل نبضة إضاءة. كذلك، أظهرت النتائج زيادة في التيار الضوئي مع زيادة محتوى أوكسيد المعدن في المتراكبات النانوية للبولي أنيلين مع تحسن في قيم الاستجابية، والكشفية، وغيرها من معلمات الاستجابة الطيفية.

كشفت الخصائص الأستشعارية للغاز لأغشية البولي أنيلين وأوكسيدات المعادن ومتراكباتهم النانوية عن زيادة في تحسسية الأغشية عند تعريضها لغاز الأمونيا (NH_3). أذ أظهرت النتائج نقص في قيم زمن الأستجابة مع زيادة محتوى أوكسيد المعدن في أغشية المتراكبات النانوية للبولي أنيلين. أن أعلى تحسسية تم الحصول عليها كانت لأغشية المتراكبات النانوية المحضرة من ٥ مل من البولي أنيلين مع ٥ مل من المغنتايت و٥ مل من البولي أنيلين مع ٥ مل من المغنتايت، اذ بلغت ٢٠,٥٪ و١٨,٤٩٪ على التوالي، مقارنة بقيم التحسس للأغشية المحضرة الأخرى. سجلت أغشية أوكسيد الكوبالت واوكسيد الحديد تفوقا على بقية العينات المحضرة الأخرى، اذ أظهرت أعلى حساسية مقدارها (٦٤٦,٣٩٪) و (١٦٦,٣٦٪) على التوالي.

جمهورية العراق
وزارة التعليم العالي والبحث العلمي
جامعة ديالى
كلية العلوم
قسم الفيزياء

تطوير وتوصيف المتراكبات النانوية للبولي أنيلين - أكاسيد الحديد والكوبالت والمنغنيز لتطبيقات التحسس الغازي والكشف الضوئي

أطروحة مقدمة إلى

مجلس كلية العلوم - جامعة ديالى، وهي جزء من متطلبات نيل درجة الدكتوراه فلسفة

في علوم الفيزياء

من قبل

مهدي حاتم ديوان

بكالوريوس علوم في الفيزياء ١٩٩٩ م

ماجستير علوم في الفيزياء ٢٠٠٢ م

إشراف

أ.د. نبيل علي بكر

أ.د. عصام محمد ابراهيم

١٤٤٦ هـ

٢٠٢٥م